AEP 4900 Final Report, Fall 2018

1 Introduction

The physical mechanism underlying polarization in ferroelectric materials is the spontaneous displacement of ions from their equilibrium positions in the unit cell. In the perovskite oxides, polarization is largely due to the displacement of the B-site cation relative to the rest of the unit cell. In a macroscopic sample, a ferroelectric material will have finite regions of uniform polarization known as domains. When two such regions of differing polarization meet, the interface is what is known as a domain wall. While the allowed directions of the polarization within a domain are largely determined by the symmetry of the material's crystallographic point group, the way in which the polarization direction transitions between two domains is by no means as obvious. In general, crystal symmetry, defects, strain coupling, and finite size factors such as sample thickness or electrostatic boundary conditions will all have an effect on the energy landscape governing the domain wall's character. This can result in novel order parameter topologies at the domain wall interface.

Unlike bulk property measurements, real-space atomic-resolution imaging techniques, such as scanning transmission electron microscopy (STEM) hold the capability of resolving the change in polarization direction between domains, atom by atom. STEM has an advantage over scanned probe techniques in that its large field of view and variable magnification allows one to locate the positions of domains and domain boundaries across a macroscopic sample before taking an atomic resolution mapping. Indeed, much work has been done using STEM and picometer precision tracking to map the displacements of ions relative to a lattice in room temperature ferroelectrics[1].[5]

My research this semester fits underneath the broader goal of extending these techniques to study materials at cryogenic temperatures and gain access to access to novel low temperature phases. While cryogenic STEM at atomic resolution has long remained difficult due to issues with sample drift and sample holder stability during image acquisition, recent work[6] has provided a viable means of aligning rapid acquisition scans in post processing, making a study of this nature feasible.

As a specific system, I have studied barium titanate (BTO) which undergoes a structural phase transition to a low temperature rhombohedral phase when cooled to liquid nitrogen temperatures. Computational work suggests that the this phase may host mixed character domain walls and interesting topological defects[38].[7] Here I report progress done to identify and characterize domain walls in BTO's room temperature phase using differential phase contrast (DPC)-STEM. Not only does DPC-STEM allow for the location of ferroelectric domains, but it serves as a complementary technique for measuring in plane components of polarization. This work will ultimately serve to provide a benchmark of comparison for future experiments done at cryo.

2 Sample Preparation

The sample used for the experiment was polycrystalline barium titanate grown by Sang-Wook Cheong's group at Rutgers. A section was cut from the bulk polycrystal using a diamond saw and flat polished to a high surface quality using diamond paper up to 0.1μ grade. The sample was then

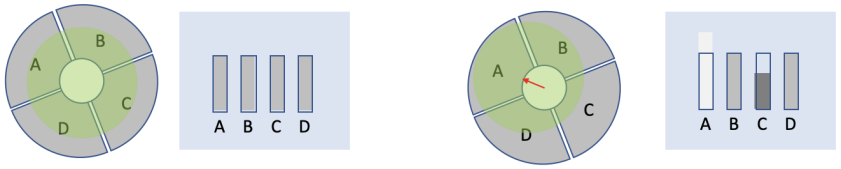

Figure 1: Pictographic explanation of differential phase contrast imaging: Prior to imaging, the CBED pattern must be aligned such that it sits evenly on all detectors, and gain offset must be equalized. Reading out differential signals from opposing quadrants lets us map shifts in the BF disk COM across the sample.

sputter-coated with amorphous carbon to avoid charging in the SEM and colloidal silver paint was applied along the edges to account for shadowing effects in the sputter deposition process.

To map grain orientation across the sample, electron back scatter diffraction (EBSD) was performed on a Tescan Mira3 FESEM with an incidence angle of 70 degrees and an operating voltage of 20kV. A 512x512 map of a 200μm region was acquired over the course of two hours.

From the resulting stereographic projection dataset, orientation of the principle axes relative to the plane of the image was determined. An optimally aligned grain was identified and extracted using standard FIB lift out techniques on an FEI Strata 400 FIB. From the EBSD data set, it was determined that the FIB cut was taken 14.9° from the [001] zone axis. It was later found that when inserted into the TEM using a a double tilt holder, tilt angles of $\alpha = 17.9°$ and $\beta = 0°$ were needed to bring the sample on axis. This shows that the EBSD mapping was accurate to within 3°, which is suitably precise for the tilt ranges accessible by our sample holders.

In hindsight, this procedure could be streamlined by decreasing the sampling frequency when searching for a suitable area in a wide field of view. Shorter net acquisition times also raise the possibility of using less if not no amorphous carbon, which would yield sharper data as well as more precise indexing by the Bruker Quantax software package.

3 Experimental Methods

Differential phase contrast imaging and high-angle annular dark-field imaging was performed in an aberration-corrected scanning transmission electron microscope (FEI Titan Themis) at 300kV. A segmented DF4 Thermo Scientific detector in the back focal plane was used in conjunction with FEI's Velox software to read out differential signals from opposing quadrants. From this, orthogonal components of the central diffraction disk's center-of-mass shifts were measured as the beam was scanned across the sample (Figure 1).

Prior to imaging the, the convergent beam electron diffraction (CBED) pattern was centered equally on all 4 quadrants. Their gain offsets were then adjusted to give equal readout in the presence of no sample. When the electron beam of the microscope interacts with an electrically polarized sample, it feels the Lorenz force of the displaced cation such that the beam's center of mass is deflected in the same direction as the polarization (the same principle applies to a ferromagnetic material, in which the deflection occurs due to the inherent magnetization). This, in principle, lets

us map order parameters of the sample with this differential phase contrast technique. However, phase contrast may also arise from a number of other sources such as strain, thickness, surface contamination, or induced charging, so care must be taken when interpreting signal readout.[2] Unlike Lorenz TEM which works at large defocus, DPC operates at in focus optical conditions, making it relatively straight forward to switch between DPC and HAADF imaging modes.

In order to visualize the total in plane component of the electric polarization, I wrote python code to combine the two differential readout signals vectorally into one HSV map where a singled valued hue encodes the polarization direction at a given pixel and brightness encodes the overall magnitude. This is similar to a technique employed in.[2] My code uses the hyperSpy package to read in data from the Velox .emd format and the openCV package for image processing. FEI Velox files are stored as .emd files, which are essentially proprietary wrappers for the more general '.hdf5' format.[4] While .emd files can be read in using any standard .hdf5 reader, hyperSpy has the advantage that the original metadata can be easily read out which makes handling the peculiarities of this proprietary format considerably easier.

4 Results and Analysis

Before DPC Imaging, the overall structure of the sample was characterized (Figure 2). Even within a single grain extracted using FIB, there was a significant concentration of defects. Most notably, the FIB sample itself had a macroscopic crack running through it. This was present in the sample before it was even removed from the FIB, as shown in the SEM image (Figure 2 (f)). Examination of the CBED pattern on either side of the crack showed the crystallographic orientation to be nominally the same, indicating that this was not in fact a grain boundary, but simply a crack. At low magnification, moiré patterns (Figure 2 (d),(e)) indicated regions with edge dislocations (d) as well as regions relatively free of defects (e). Since moiré patterns are an aliasing effect, broken periodicity of the lattice at the atomic level through edge dislocations will be reflected in the moiré pattern at lower magnifications. Further examination of the sample using HAADF imaging (Figure 2 (a),(b), (c)) supports this conclusion. The region imaged in (a) is relatively free of defects and the peaks in its FFT are point-like and well defined. In contrast, the region imaged in (b) contains several defects and its FFT shows peak blurring and splitting, indicating slight deviations from perfect periodicity. This relatively high concentration of defects in our sample is noteworthy in the context of trying to understand its ferroelectric domain structure. Theoretical and computational models of ferroelectric domain structure assume perfect crystallinity. In this approximation, the assertion that ferroelctric displacements will be constrained entirely to symmetry preferred directions is valid, but the further we stray from a perfect crystal in our real material, the less valid this argument becomes.

Before we try to interpret our DPC datasets, it helps to consider the possible configurations of domains and domain walls, and what sort of differential readout maps you would expect from them. There are several things which simplify this sort of conceptual treatment. First off , polarization well within each domain is confined to lie along the symmetry allowed directions of the underlying crystal lattice. This lets us decouple the domain structure problem into the polarization direction of the domains themselves and how this polarization direction changes across domain walls. In BTO's room temperature tetragonal phase, the polarization is confined to be parallel with the basis vectors. This implies that our domains must lie at either 90° or 180° from one another. To simplify the following discussion, we assume that our domains align with our detector quadrants

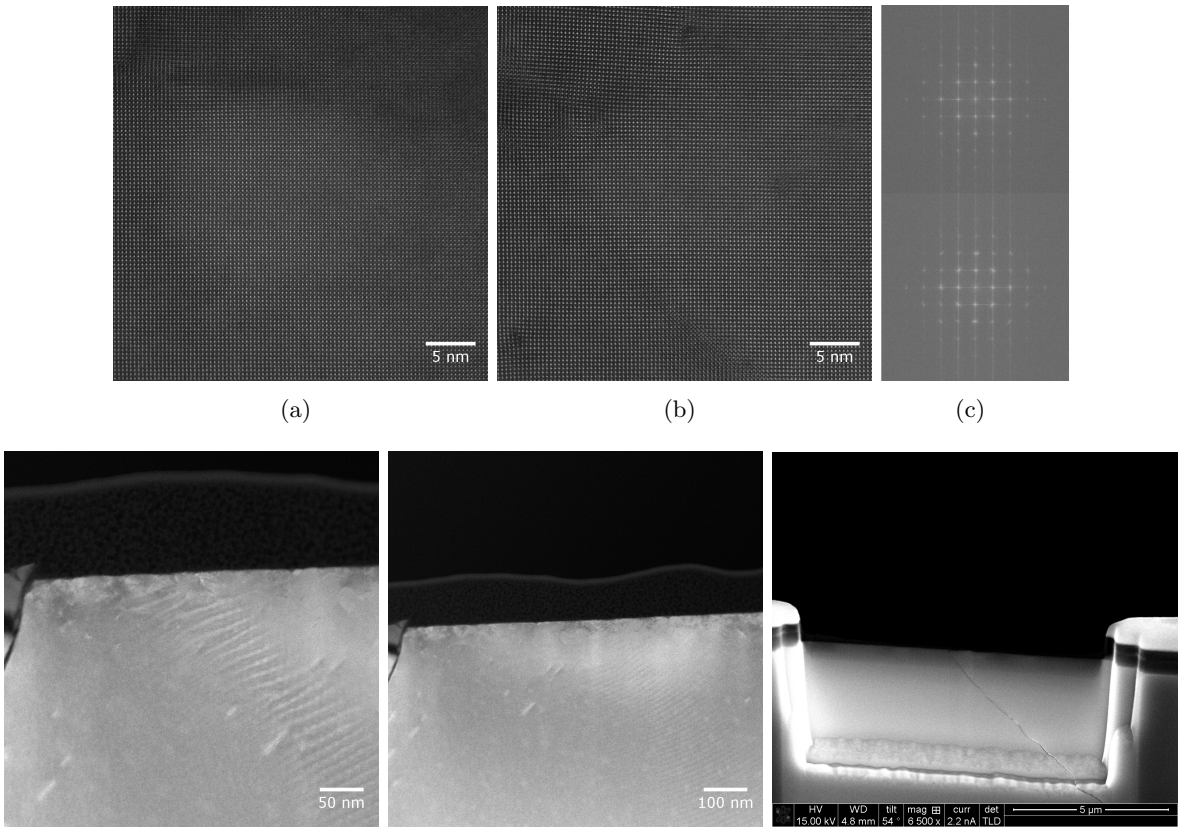

(a) (b) (c)

(d) (e) (f)

Figure 2: Sample Overview: (a) HAADF acquire of an area of the sample that was largely free of crystal deffects. (b) HAADF acquire of an area of the sample that contained ¡¿ deffects. (c) FFT's of a,b. Note the peak broadening and splitting in b's FFT indicative of structural deformation. (d),(e) low mag moiré contrast across the sample (f) SEM image from FIB showing cracked region that was extracted

(or intersect them at 45°, since signals from rotations thereafter can easily be inferred as linear combinations of the diagrams below. For these two allowed angles, we may have either head to tail or head to head alignment, giving 4 potential domain configurations (Figure 3). Theory predicts that the head to head configurations would not be observed since they are energetically unfavorable but we include them anyways for discussion purposes.

The simplest model for domain structure is the Ising model, where the polarization simply dies out between domains. Hence, in the case of Ising domains the expected DPC map would look exactly like that of our allowed domain structures (Figure 3). More complicated models allow for the polarization vector to rotate across the domain wall instead of dying off. In the Neel model, this rotation happens in the plane of polarization, where as in the Bloch model this occurs out of the plane. Figures 4, 5 depict thes cases.

Note how for several of these cases, there is more than one equally prefferable domain wall configuration. This sort of frustration could lead to, in general, aperiodic domain wall structures across the sample. Also, keep in mind that understanding the domain structure is inherently

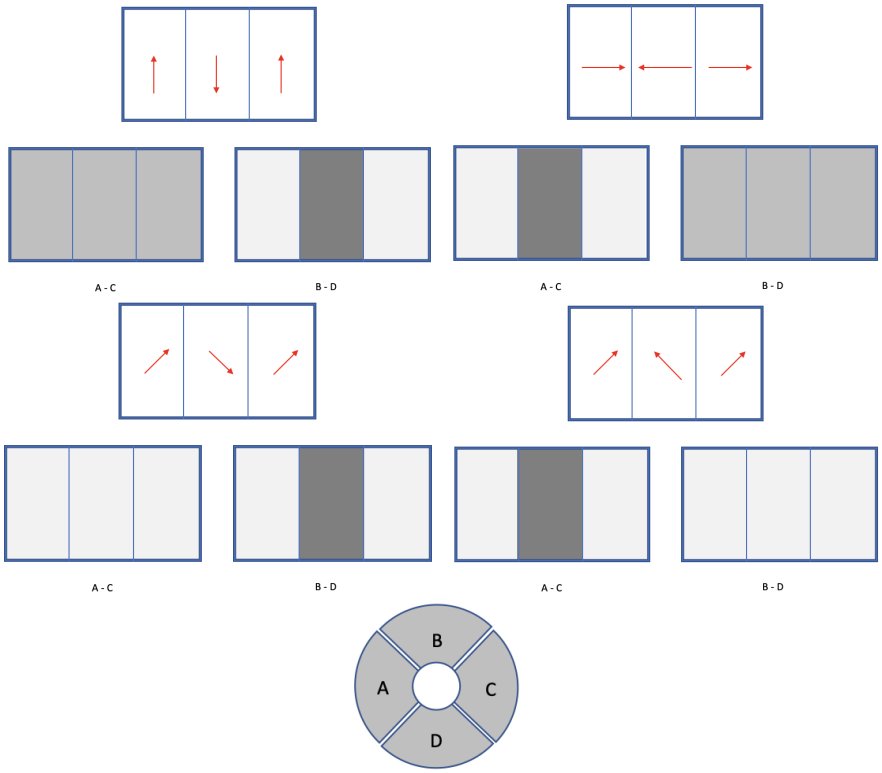

Figure 3: Possible domain configurations for BTO and their corresponding differential signal readouts. In the case of Ising domain walls, where polarization dies off at the interface, this would simply be the expected differential readout.

a 3D problem. Experimentally, we only have access to a down-axis projection of our domain configuration, which means that if there is any polarization perpendicular to our field of view, we will not be able to observe it with this technique alone. This is especially relevant for the Bloch type domain walls where the projection image would be completely indistinguishable from that of an Ising type wall. In general our domain walls may also be of mixed character and have combinations of features from each of these simple models.

We are now ready to analyze and interpret our differential readout maps from DPC. Figure 6 shows a domain wall structure at 115kx magnification. The first line plot profile can be largely considered as two distinct patterns with a transition occurring around the x = 300px mark. The first region exhibits a roughly constant signal in A-C interrupted by alternating spikes at the domain walls, and a step function in B-D. It is important to note that the significant domain wall contribution in the A-C signal implies that a simple Ising picture of the domain structure is inadequate in this situation. What this pattern is consitent with, however, is the our picture of a Neel domain structure as in the top right diagram of Figure(4) or alternatively the out of plane component of a Bloch structure as described in the left picture of Figure 5. The second line plot profile exhibits this same behavior even more distinctly. The limitation of a projection image is that there is no way to determine from these signals individually whether the rotation is in plane or out of plane. The behavior in the first line profile plot is distinctly different. In this case, the A-C signal picks up a step function behavior in the domains in addition to the spikes along the

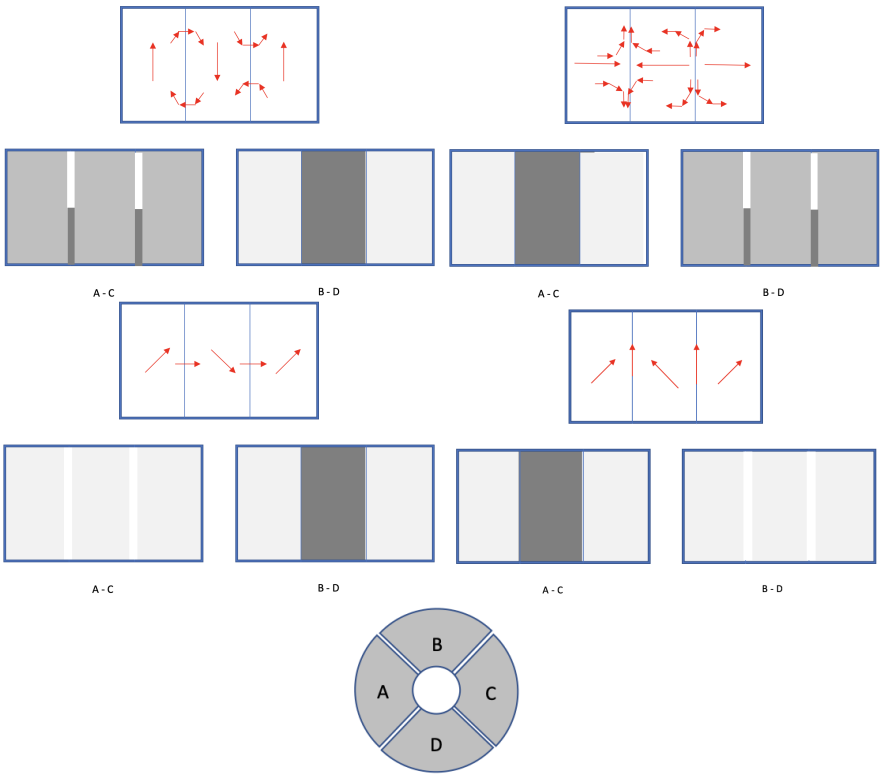

Figure 4: Possible differential readout maps for the case of Neel type (in plane polarization rotation) domain walls. Note that for some cases, there is more than one possible domain wall configuration. Remember that the right cases are not energetically preferable.

domain walls. This behavior is not directly interpetable in terms of linear combinations of any of our basic models. In fact, a polarization which transitions by growing at the domain walls is not physically reasonable. Figure 7 displays this same behavior but at a higher magnification.

These disjoint differential mappings and plot profiles do not provide a satisfactory explanation of the domain behavior in either case, the first because we cannot resolve whether the polarization occurs in plane (Neel) or out of plane (Bloch), and in the second case because it seems to imply a polarization transition that is not physically reasonable. To resolve these discrepancies, I employed the color mapping code that I wrote, producing the images in Figure 8. While physically meaningful, these color plots are currently rather limited in their current capabilities. Both images suffer from a number of issues that obfuscate the underlying polarization field. First, both images sufer from color noise. This is unavoidable due to the nature of subtracting two large signals from one another. Second, DPC picks up from contrast from tilt, thickness, and strain. The tilt and thickness can be seen in a monotonic variation in contrast that goes from the upper left to lower right of the sample. In the second image, the strain termination at the interface stongly dominates the signal. While there should be ways to filter these signals out, care must be used in order retain the physical meaning of the underlying signal. Finding a way to do this would be a good task for future work on this project. All this said, the plot of the higher magnification region does provide a degree of insight into what we saw as an nonphysical polarization transition. Upon close inspection of the domain wall structures, there is a distinct fine color splitting, red-green in one case, blue-pink

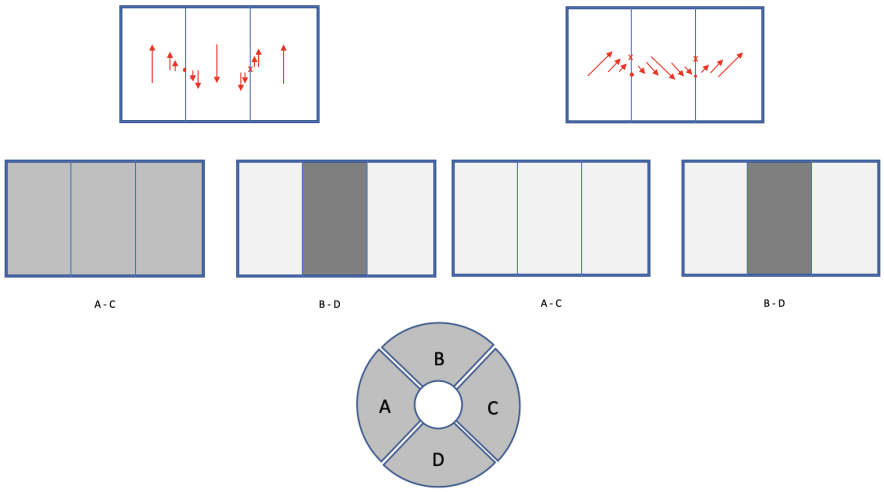

Figure 5: Possible differential readout maps for the case of Bloch type (iout of plane polarization rotation) domain walls. Note how the detector signal is indistinguishable from that of an Ising wall. Only two configurations are shown because head to head domains cannot be connected by a pure Bloch domain wall.

in the other. My best explanation for this behavior of distinct domains separated by split domain walls is the case of a charged 180 degree head to head or tail to tail domain wall. Although this is supposedly energetically unfavorable, it would adequately describe the peculiar domain transition we observe. With a head to head or tail to tail domain wall, we would expect a slight accumulation or depletion of charge at the interface. This accumulation or depletion would result in an electric field emanating inward or outward on either sides of the domain wall and would result in a signal in our DPC readout. This behavior was observed by[2] in bismuth ferrite, and is remarkable that it is evidently found here in barium titanate as well.

5 Conclusion and Outlook

A domain structure that is not easily interpreted in terms of a simple Ising structure is exciting and warrants further consideration as well as analysis by complementary experimental techniques.

he next obvious choice of technique to further characterize the sample would be to employ atomic resolution imaging along with picometer precision atom tracking. High resolution HAADF images and stacks were acquired across a domain wall, but at the moment are unable to be registered. Figure 9 shows several attempts at registration. Circular Gaussian masks with cutoff parameters n = 0.5, 1, 2, 3, 4, 5, 6 were attempted, and the 2, 3, 4 masks showed the most promising results. Whereas the n = 4 mask succeeds in registering the A-sites, it completely blurs out the B-site contrast from which polarization could be determined. It's shift matrix also lacks continuity, a clear sign that it is not a physically reasonable registration. While the n = 2 and 3 images have marginally better shift matrices, their averaged images are visually poorer. A n=1 (not pictured) mask offered no improvement in shift matrix quality and produced an even more blurred image. Going forward, I will attempt to register these images using different mask shapes as desribed in[6] in order to best leverage the frequency information in the sample.

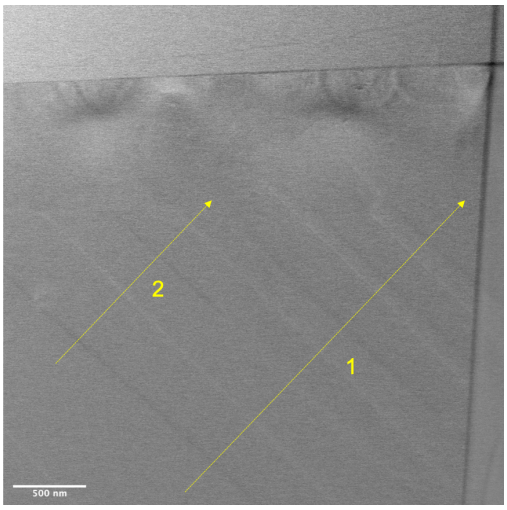

(a) A-C

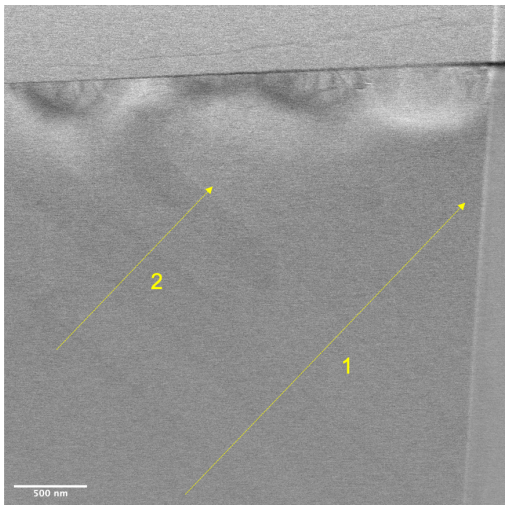

(b) B-D

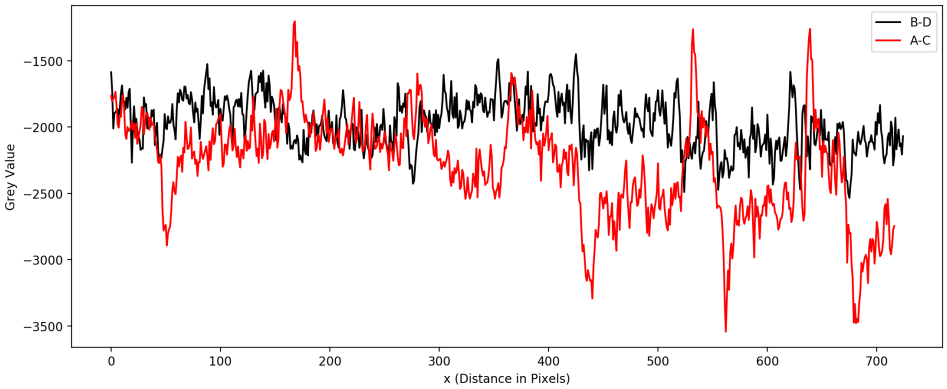

(c) Line Plot Profile 1

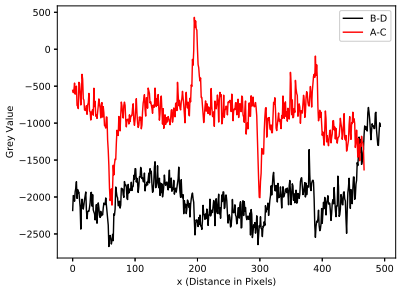

(d) Line Plot Profile 2

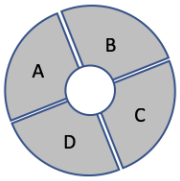

(e) Detector Orientation

Figure 6: DPC differential readout maps and line profiles over the entire FIB lamella at 29kx

References

[1] Chun-Lin Jia, Knut W. Urban, Marin Alexe, Dietrich Hesse, and Ionela Vrejoiu. Direct Observation of Continuous Electric Dipole Rotation in Flux-Closure Domains in Ferroelectric

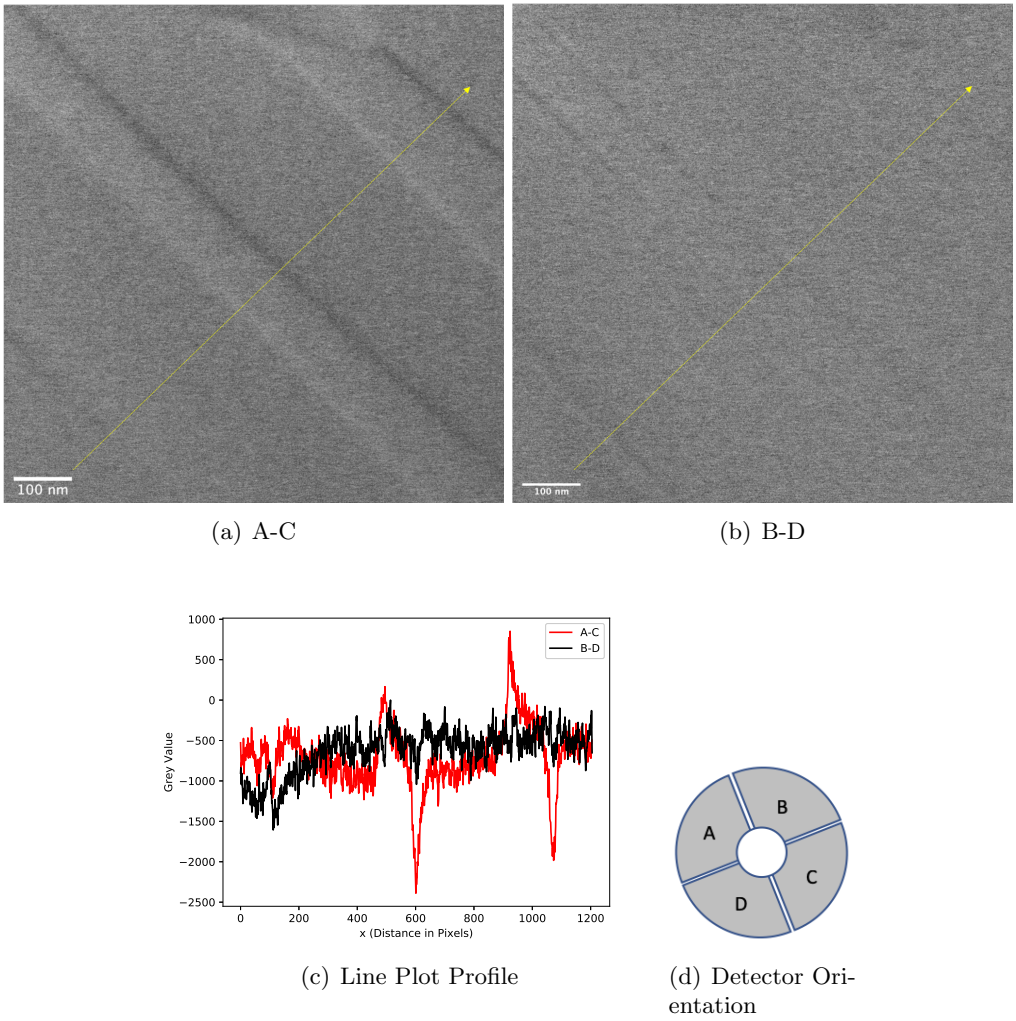

(a) A-C

(b) B-D

(c) Line Plot Profile

(d) Detector Orientation

Figure 7: DPC differential readout maps and line profiles over a domain structure at 115kx.

Pb(Zr,Ti)O3. *Science*, 331(6023):1420–1423, March 2011.

[2] Ian MacLaren, LiQiu Wang, Damien McGrouther, Alan J. Craven, Stephen McVitie, Roland Schierholz, András Kovács, Juri Barthel, and Rafal E. Dunin-Borkowski. On the origin of differential phase contrast at a locally charged and globally charge-compensated domain boundary in a polar-ordered material. *Ultramicroscopy*, 154:57–63, July 2015.

[3] P. Marton, I. Rychetsky, and J. Hlinka. Domain walls of ferroelectric ${\text{BaTiO}}_{3}$ within the Ginzburg-Landau-Devonshire phenomenological model. *Phys. Rev. B*, 81(14):144125, April 2010.

[4] Colin Ophus. Electron Microscopy Datasets | An HDF5-based interchange file format for electron microscopy data and metadata.

[5] Jonathan J. P. Peters, Geanina Apachitei, Richard Beanland, Marin Alexe, and Ana M. Sanchez. Polarization curling and flux closures in multiferroic tunnel junctions. *Nature Communications*, 7:13484, November 2016.

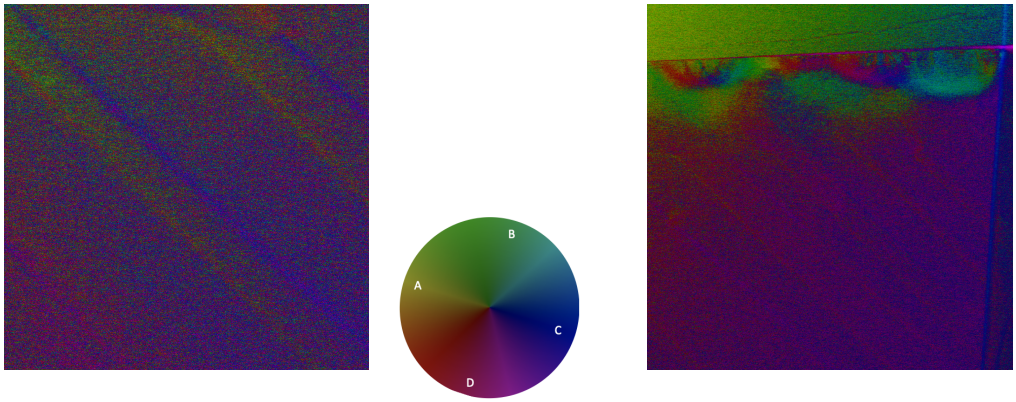

(a) (b) (c)

Figure 8: Color mapping of polarization orientation. Hue corresponds to angle, brightness to magnitude. The same code used to map the images was used to create the color wheel, a testament to its validity.

[6] Benjamin H. Savitzky, Ismail El Baggari, Colin B. Clement, Emily Waite, Berit H. Goodge, David J. Baek, John P. Sheckelton, Christopher Pasco, Hari Nair, Nathaniel J. Schreiber, Jason Hoffman, Alemayehu S. Admasu, Jaewook Kim, Sang-Wook Cheong, Anand Bhattacharya, Darrell G. Schlom, Tyrel M. McQueen, Robert Hovden, and Lena F. Kourkoutis. Image registration of low signal-to-noise cryo-STEM data. *Ultramicroscopy*, 191:56–65, August 2018.

[7] V. Stepkova, P. Marton, and J. Hlinka. Ising lines: Natural topological defects within ferroelectric Bloch walls. *Phys. Rev. B*, 92(9):094106, September 2015.

[8] Maryam Taherinejad, David Vanderbilt, Pavel Marton, Vilgelmina Stepkova, and Jiri Hlinka. Bloch-type domain walls in rhombohedral BaTiO${}_{3}$. *Phys. Rev. B*, 86(15):155138, October 2012.

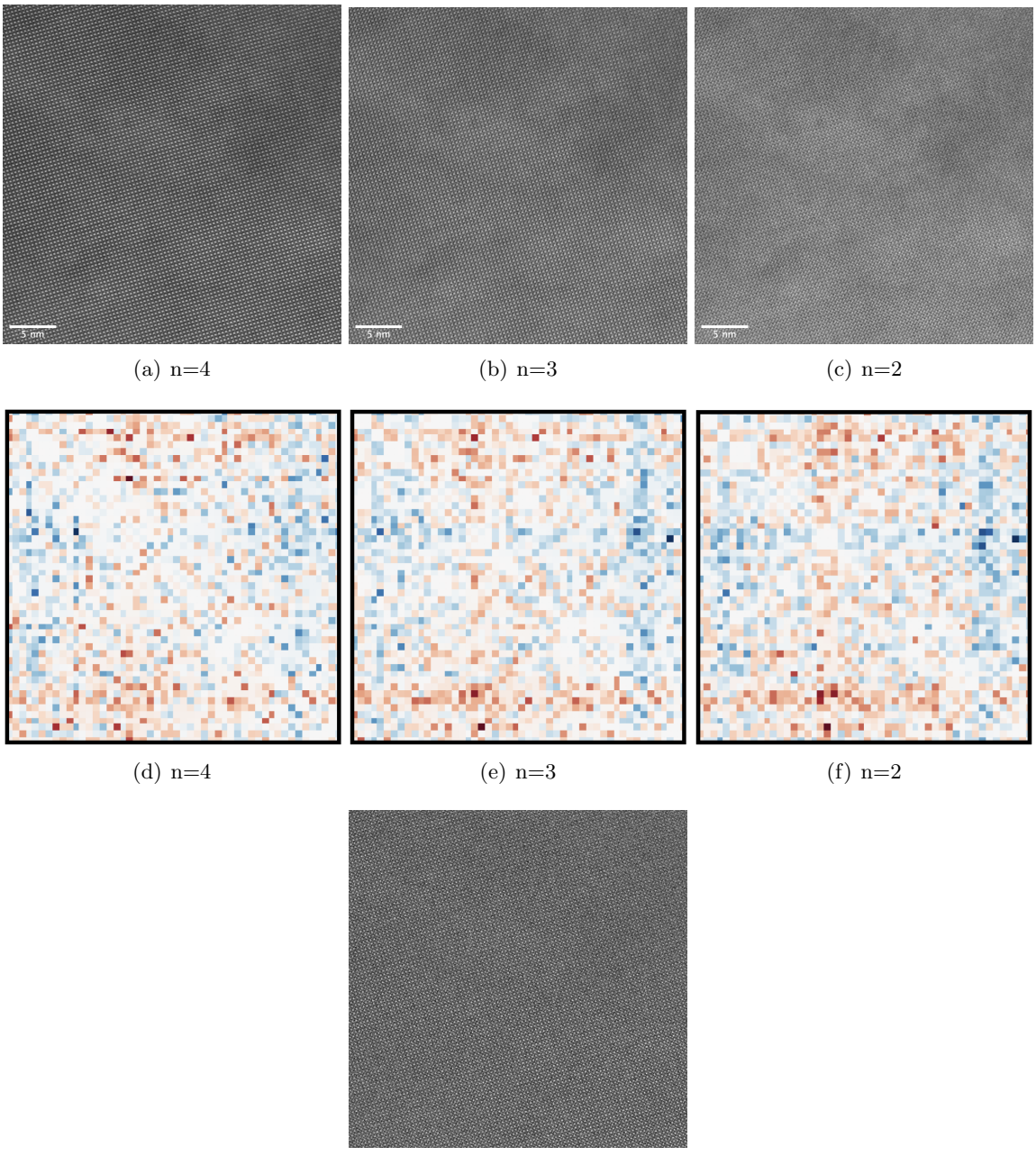

(a) n=4 (b) n=3 (c) n=2

(d) n=4 (e) n=3 (f) n=2

(g)

Figure 9: (a),(b),(c) Attempts at image registrations (d),(e),(f), and their corresponding shift matrices. (g) Representative single image from the stack acquire. Note the feint B-site contrast which should appear strongly in a correctly registered average.